analytical chemistry

pubs.acs.org/ac

Article

Vanin-1-Activated Fluorescent Probe for Real-Time *In Vivo* Imaging of Inflammatory Responses Across Multiple Tissue Types

Dianfeng Dai, Zhimin Zhang, Mo Ma, Jingkang Li, Siqi Zhang, Pinyi Ma,* and Daqian Song*

Cite This: *Anal. Chem.* 2025, 97, 1402−1409

Read Online

ACCESS | Metrics & More | Article Recommendations | Supporting Information

ABSTRACT: Vanin-1 is a pantetheine hydrolase that plays a key role in inflammatory diseases. Effective tools for noninvasive, real-time monitoring of Vanin-1 are lacking, largely due to background fluorescence interference in existing probes. To address this issue, we developed a dual-modal fluorescent and colorimetric probe, MB-Van1, to detect Vanin-1 with high sensitivity and selectivity. MB-Van1 has a structure optimized to exhibit nearly zero background fluorescence, resulting in a high signal-to-noise ratio that enables the accurate detection of Vanin-1 activity in various biological tissues. *In vitro* experiments demonstrated that MB-Van1 had a detection limit as low as 0.031 ng/mL in the fluorescence mode. We successfully employ MB-Van1 to observe elevated Vanin-1 levels in inflammatory tissues of various mouse models of rheumatoid arthritis (RA), drug-induced liver injury (DILI), and nonsteroidal anti-inflammatory drug (NSAID) enteropathy models, within only 5 min. This advancement provides a novel approach for monitoring the dynamic changes of Vanin-1 during inflammation, offering new strategies for the early diagnosis and therapeutic assessment of other related diseases.

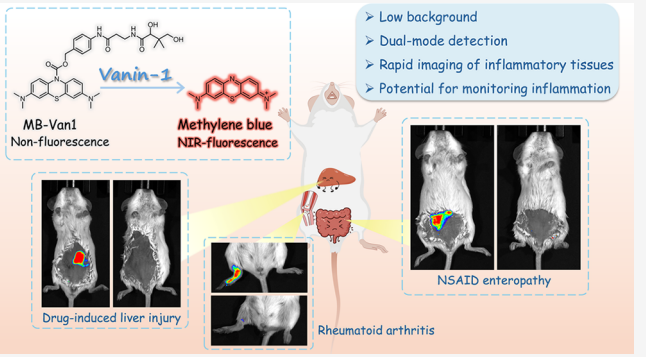

INTRODUCTION

Inflammation represents a self-protective response of the body to harmful stimuli, including pathogen invasion, physical injury, or chemical irritation.[1−3] It involves complex cellular and molecular mechanisms.[4,5] Disease biomarkers are critical for elucidating the mechanisms underlying inflammation, diagnosing inflammatory conditions, and evaluating therapeutic efficacy.[6−8] Although traditional diagnostic methods such as blood tests and histological examinations are effective, they inevitably cause harm to organisms to some degree.[2,9,10] In contrast, fluorescent probes offer the advantage of non-invasiveness, allowing for the direct labeling and tracking of key molecules involved in inflammation, thereby facilitating real-time visualization of inflammatory activity within deep tissues.[11−15] However, the inherent background fluorescence associated with these probes can interfere with the diagnosis, thereby limiting their broader application.[16,17]

Vanin-1, a glycosylphosphatidylinositol (GPI)-anchored enzyme with pantetheinase activity, is ubiquitously expressed in various organs, including the liver, intestine, and kidney.[18−21] Recent studies have highlighted the significant potential of Vanin-1 as a disease biomarker, showing its close association with the progression of multiple diseases such as acute kidney injury, inflammatory bowel disease, diabetes, and influenza.[22−27] Vanin-1 influences CoA metabolism by catalyzing the hydrolysis of pantetheine to cysteamine and pantothenate, which subsequently regulate the intracellular redox status and glutathione levels.[28,29] These alterations are intimately linked to the onset and progression of inflammation.[30] Despite the growing clarity regarding Vanin-1's role in inflammation, there are challenges in the direct, real-time monitoring of its activity at inflammatory sites *in vivo* still persist.[31] To date, only Ma et al. have successfully employed a fluorescent probe technology to visualize intestinal Vanin-1 activity in a mouse model of inflammatory bowel disease (IBD).[32] Although this represents a significant milestone, it fails fully address the broader research and application needs. Consequently, there is a need for a fluorescent probe capable of efficiently and accurately detecting Vanin-1 activity across various biological tissues.

In response to this challenge, we developed an MB-Van1 probe. The probe was synthesized by integrating the fluorophore methylene blue with the recognition group pantothenate using 4-aminobenzyl alcohol as a self-eliminating linker. The disruption of methylene blue's conjugated structure resulted in MB-Van1 having nearly zero background fluorescence, which led to the significant enhancement in its signal-to-noise ratio for fluorescence imaging in complex

Received: November 6, 2024
Revised: January 2, 2025
Accepted: January 3, 2025
Published: January 9, 2025

https://doi.org/10.1021/acs.analchem.4c05982
Anal. Chem. 2025, 97, 1402−1409

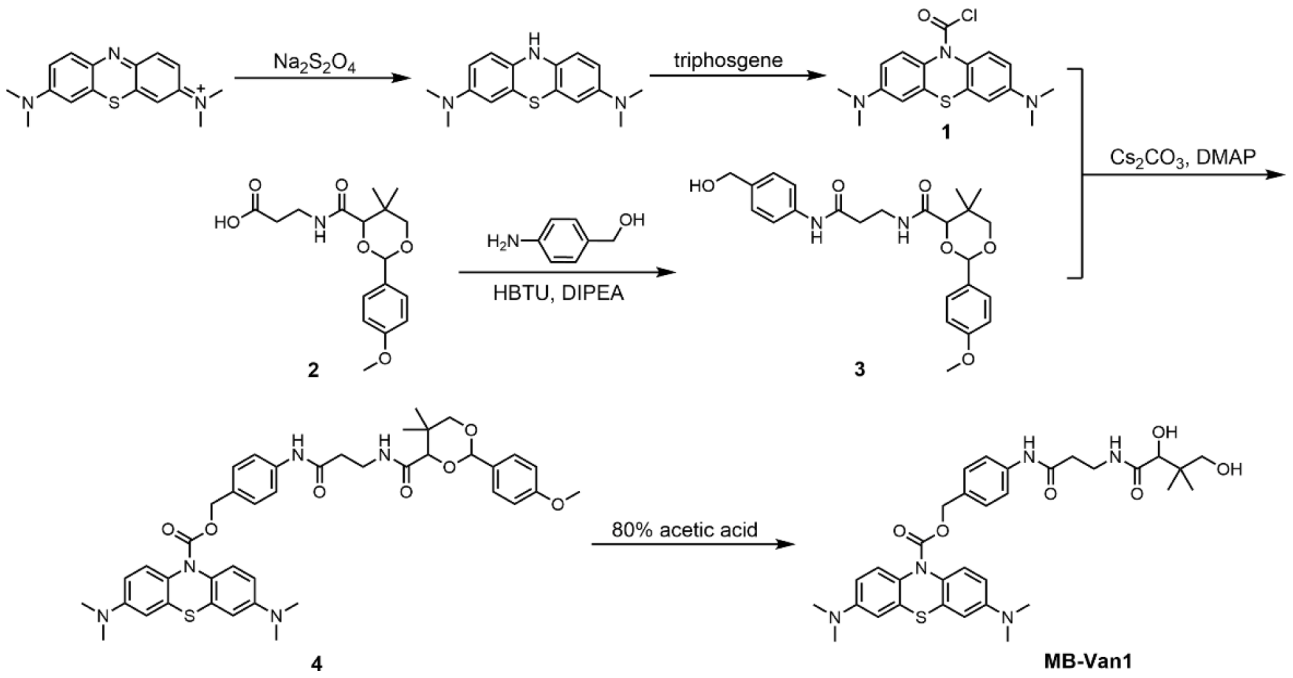

Figure 1. Synthesis route of MB-Van1.

biological systems. The high sensitivity and specificity of the MB-Van1 probe enabled us to achieve precise fluorescence imaging of inflammatory tissues in a variety of mouse models including drug-induced liver injury, NSAID enteropathy, and rheumatoid arthritis models. This study not only provides novel diagnostic and monitoring tools for inflammatory diseases but also contributes to the understanding of dynamic changes in Vanin-1 during the inflammatory process. It also offers new insights that are beneficial to mechanistic research and therapeutic strategies.

EXPERIMENTAL SECTION

Materials and Instruments. The specific materials and equipment employed in this study are detailed in the Supporting Information.

Synthesis. The synthetic route for the MB-Van1 probe is illustrated in Figure 1. The syntheses of Compound 1, Compound 2, and Compound 3 have been described in the literature.[33,34]

Synthesis of Compound 4. Under a nitrogen atmosphere, compound 1 (177 mg, 0.51 mmol), compound 3 (204 mg, 0.46 mmol), Cs_2CO_3 (487 mg, 1.38 mmol), and DMAP (56 mg, 0.46 mmol) were dissolved in 20 mL of CH_2Cl_2, and the components were allowed to react at 45 °C overnight. The reaction progress was monitored using thin-layer chromatography (TLC) until completion. The mixture was washed three times with 50 mL of 1 M HCl, and the solvent was subsequently removed by vacuum distillation. The resultant crude intermediate was directly used in the subsequent reaction without further purification.

Synthesis of MB-Van1. Compound 4 (40 mg, 0.054 mmol) was dissolved in 80% acetic acid and stirred at room temperature for 3 h. The reaction mixture was then concentrated under a reduced pressure to remove the solvent. The resulting crude product was purified by silica gel column chromatography using a CH_2Cl_2/CH_3OH mixture (*v*/*v*, 10:1) as the eluent, which yielded MB-Van1 as a light blue solid (23 mg, 67% yield). ^{1}H NMR (600 MHz, $CDCl_3$) δ 8.49 (s, 1H), 7.48 (d, J = *8.4 Hz*, 2H), 7.35 (d, J = *8.5 Hz*, 2H), 7.25 (d, J = *8.4 Hz*, 2H), 6.71 (s, 2H), 6.65 (d, J = *6.8 Hz*, 2H), 5.17 (s, 2H), 4.00 (s, 1H), 3.62−3.58 (m, 2H), 3.50 (s, 1H), 3.47 (t, 2H), 2.92 (s, 12H), 2.55 (t, J = *5.9 Hz*, 2H), 2.10 (s, 1H), 0.91 (s, 6H) (Figure S1).^{13}C NMR (151 MHz, $CDCl_3$) δ 174.26, 174.05, 170.00, 154.57, 137.70, 132.91, 132.25, 128.49, 127.08, 120.02, 111.54, 110.80, 77.51, 70.82, 67.47, 40.98, 39.33, 36.79, 35.23, 20.52 (Figure S2). HR-MS (*m*/*z*): Calculated for $[C_{33}H_{42}N_5O_6S]^+$: 636.2778, found: 636.2766 (Figure S3).

***In Vitro* Detection of Vanin-1.** The MB-Van1 probe was dissolved in DMSO to prepare a 1 mM stock solution. The final reaction, with a total volume of 1 mL, consisted of MB-Van1 (10 μM), PBS (10 mM, pH 7.4), and the analyte. The reaction mixture was incubated in a shaking incubator at a constant temperature of 37 °C for 40 min prior to spectroscopic analysis. The UV−vis absorption and fluorescence spectra of the reaction mixture were measured using a 1 cm quartz cuvette.

Cell Imaging of Endogenous Vanin-1. Cells used for imaging studies were divided into six groups. The first group served as the control with untreated cells. The second group was treated with MB-Van1 (10 μM) for 30 min before imaging. The third group was pretreated with RR6 (50 μM) for 2 h, followed by incubation with MB-Van1 (10 μM) for 30 min prior to imaging. The fourth to sixth groups were treated with different concentrations of LPS (20, 50, and 200 μg/mL, respectively) for 24 h, followed by incubation with MB-Van1 (10 μM) for 30 min. For all groups, cells were washed three times with PBS (10 mM, pH 7.4) prior to imaging. Imaging was performed with excitation at 640 nm and emission collected between 663 and 738 nm.

Fluorescence Imaging of Mouse Models. All animal experiments were conducted with the approval of the Institutional Animal Care and Use Committee (IACUC) of Jilin University, under the ethics review permit number

https://doi.org/10.1021/acs.analchem.4c05982
Anal. Chem. 2025, 97, 1402−1409

SY202306031, and in accordance with the established ethical protocols.

Imaging of Rheumatoid Arthritis Mouse Model. For the rheumatoid arthritis mouse model, mice in the experimental group were injected with λ-carrageenan (0.1 mg/mL, 50 μL in PBS) in the right tibiotarsal joint once daily, while those in the control group received an equivalent volume of PBS. After 1 week, all mice were subcutaneously injected with 100 μL of MB-Van1 (1 mM) in the right tibiotarsal joint. The mice were then anesthetized with isoflurane, and *in vivo* imaging was performed using a small animal imaging system 5 min postinjection.

Imaging of Drug-Induced Injury Mouse Model. For the drug-induced injury mouse model, mice were first fasted overnight. Mice in the experimental group were intraperitoneally injected with 300 mg/kg APAP, while those in the control group received an equal volume of PBS. Six hours postinjection, the hair on the abdomen of all mice was removed using depilatory cream. The mice were then injected with 100 μL of MB-Van1 (1 mM) in the tail vein. Five minutes after injection, they were anesthetized with isoflurane and then subjected to *in vivo* imaging using a small animal imaging system. Following the imaging, all mice were immediately dissected, and the dissected tissues were subjected to fluorescence imaging using a small animal imaging system.

Imaging of NSAID Enteropathy Mouse Model. Mice in the experimental group received indomethacin (20 mg/kg) dissolved in 0.5% carboxymethyl cellulose (4 mg/mL) via gavage once daily, while those in the control group were given an equal volume of normal saline. After 2 days, the hair on the abdomen of all mice was removed using depilatory cream. The mice were then intrarectally injected with 100 μL of MB-Van1 (1 mM). Five minutes postinjection, the mice were anesthetized with isoflurane and then subjected to *in vivo* imaging using a small animal imaging system. After imaging, all mice were immediately dissected, and their organs were excised for fluorescence imaging using a small animal imaging system.

RESULTS AND DISCUSSION

Design and Synthesis of MB-Van1. Methylene blue is a widely utilized and cost-effective near-infrared fluorescent dye and is well-regarded in scientific research and diagnostic applications due to its exceptional fluorescence properties.[35,36] An effective design strategy for fluorescent probes involves the modification of the nitrogen atom on the phenothiazine ring of methylene blue. The modification disrupts the original conjugated structure of the molecule, conferring the probe with the distinctive advantage of minimal background fluorescence, which significantly enhances the detection sensitivity. In this study, methylene blue was selected as the fluorophore, while pantothenic acid was used as the recognition group. These components were directly linked through a self-eliminating linker, 4-aminobenzyl alcohol, resulting in a Vanin-1-targeting fluorescent probe, MB-Van1. In its initial state, MB-Van1 was colorless and exhibited negligible fluorescence, leading to substantially reduced background interference and improved detection accuracy. Upon the presence of Vanin-1, the pantothenic acid moiety in the probe is selectively cleaved, resulting in the release of free methylene blue molecules. This cleavage transformed the color of MB-Van1 from colorless to blue, accompanied by a significant enhancement in fluorescence, thereby enabling dual-modal fluorescence and colorimetric detection of Vanin-1.

Optical Response and Reaction Condition Optimization. The spectral properties of the MB-Van1 probe were initially examined under simulated physiological conditions (pH 7.4 PBS buffer, 10 mM). MB-Van1 alone exhibited negligible UV−vis absorption; however, upon the addition of Vanin-1, a new absorption peak at 665 nm appeared. which corresponds to the absorption peak of methylene blue. The addition of Vanin-1 also resulted in the solution color change from colorless to blue (Figure 2A). Regarding the fluorescence

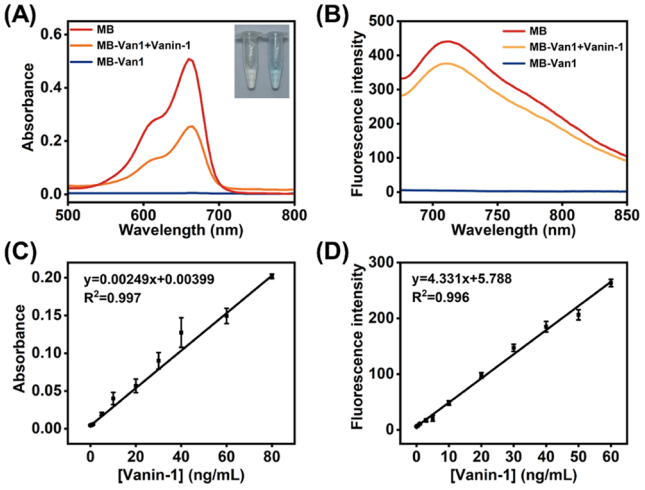

Figure 2. (A) Absorption spectra of MB-Van1 (10 μM), the reaction system (MB-Van1 + Vanin-1) and methylene blue (10 μM). The inset shows the color change of the reaction system without Vanin-1 (left) and with Vanin-1 (right). (B) Fluorescence spectra of MB-Van1 (10 μM), the reaction system (MB-Van1 + Vanin-1) and methylene blue (10 μM). (C) Linear relationship between absorbance at 665 nm and Vanin-1 concentration (0−80 ng/mL). (D) Linear relationship between fluorescence intensity (λ_{ex} = 665 nm) and Vanin-1 concentration (0−60 ng/mL).

spectra, MB-Van1 exhibited a nearly zero fluorescence background. At an excitation wavelength of 665 nm, the introduction of Vanin-1 significantly enhanced the emission peak at 710 nm. Specifically, in the presence of 200 ng/mL Vanin-1, the fluorescence intensity increased by approximately 85 folds (Figure 2B). The optical stability of MB-Van1 and its reaction system was also evaluated. Under continuous excitation by light at a wavelength of 665 nm, the fluorescence intensity remained highly stable for up to 1 h, which is indicative of excellent optical stability (Figure S4). Given that fluorescence intensity can be influenced by various environmental factors, optimization of the reaction conditions was further conducted. The data showed that the fluorescence intensity of the reaction system progressively increased with increasing reaction times, reaching the maximum value at 40 min, which was selected as the optimal reaction time (Figure S5). At pH 7.4, MB-Van1 exhibited the lowest background fluorescence and the highest fluorescence intensity; thus, pH 7.4 was selected as the optimal reaction condition (Figure S6). Additionally, after the addition of Vanin-1, the fluorescence of the reaction increased progressively at temperatures between 25 and 42 °C. Considering the physiological relevance, 37 °C was chosen as the optimal reaction temperature (Figure S7).

https://doi.org/10.1021/acs.analchem.4c05982
Anal. Chem. 2025, 97, 1402−1409

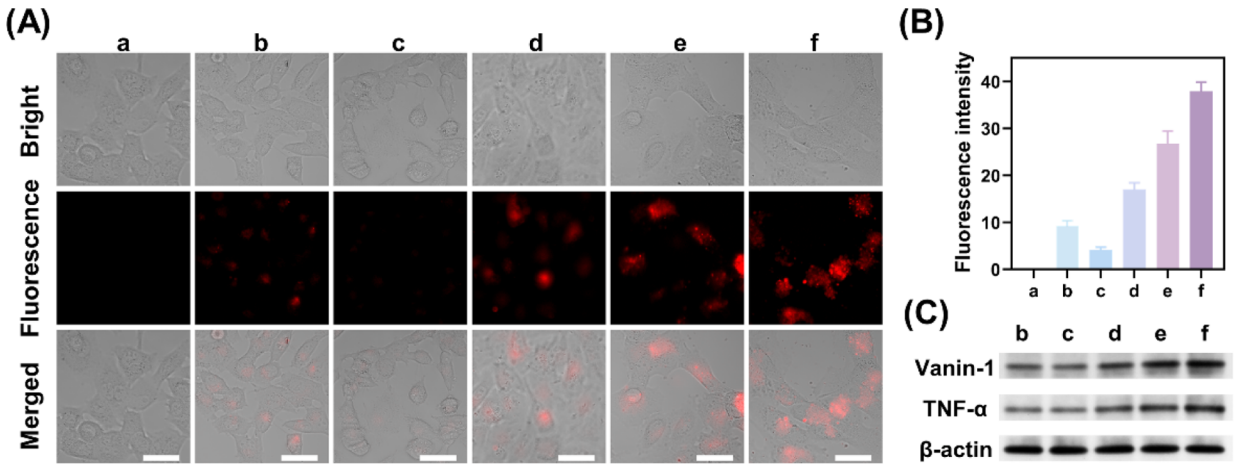

Figure 3. (A) Fluorescence imaging of LO2 cells under different treatments: (a) untreated cells; (b) cells treated with MB-Van1 (10 μM) for 30 min; (c) cells pretreated with RR6 (50 μM) for 2 h, followed by incubation with MB-Van1 (10 μM) for 30 min; (d) cells treated with LPS (20 μg/mL) for 24 h, then incubated with MB-Van1 (10 μM) for 30 min; (e) cells treated with LPS (50 μg/mL) for 24 h, followed by MB-Van1 (10 μM) for 30 min; (f) cells treated with LPS (200 μg/mL) for 24 h, followed by MB-Van1 (10 μM) for 30 min. (λ_{ex} = 640 nm, λ_{em} = 663−738 nm. Scale bar = 50 μm). (B) Comparison of fluorescence intensities of LO2 cells across different treatments as depicted in (A). (C) Western blot analysis of Vanin-1 and inflammatory marker TNF-α expression levels in the corresponding cells.

Analytical Performance. MB-Van1 enabled the quantitative detection of Vanin-1 through dual-mode fluorescence and colorimetric methods. As the concentration of Vanin-1 increased, both the absorption intensity at 665 nm and the fluorescence intensity at 710 nm of MB-Van1 increased (Figures S8 and S9). According to the colorimetric assay, the absorption intensity showed a strong linear correlation with Vanin-1 concentration at a range of 0−80 ng/mL, and the detection limit of the probe was 0.62 ng/mL (Figure 2C). Similarly, the fluorescence assay showed that the fluorescence intensity linearly correlated with Vanin-1 concentration at a range of 0−60 ng/mL, and the detection limit was as low as 0.031 ng/mL (Figure 2D). Considering that various active substances in the organism may potentially affect the probe, we conducted selective experiments on MB-Van1 (Figure S10). The results showed that the fluorescence of MB-Van1 was significantly enhanced only after binding with Vanin-1, demonstrating the potential of MB-Van1 for detection in complex biological environments.

Reaction Kinetics. The Michaelis−Menten equation was derived from the double reciprocal (Lineweaver−Burk) plot, which allows for the calculation of the Michaelis constant (K_m). The K_m for the interaction between MB-Van1 and Vanin-1 was determined to be 6.855 μM, which is indicative of a strong binding affinity between MB-Van1 and Vanin-1 (Figures S11 and S12).

Sensing Mechanism. The response mechanism of MB-Van1 to Vanin-1 was investigated using LC-MS. The mass spectrometry analysis of the reaction system revealed a peak at m/z 284.1240, which corresponded to the mass peak of methylene blue (m/z 284.1260) (Figures S13 and S14). The HPLC analysis further supported these findings, showing chromatographic peaks at 3.01 and 4.81 min, which matched the retention times of MB and MB-Van1, respectively (Figure S15). Based on these results, we may propose that the sensing mechanism of MB-Van1 involves the specific cleavage of the pantothenic acid moiety by Vanin-1. This cleavage then triggers the self-elimination of the aminobenzyl alcohol linker, resulting in the release of free methylene blue.

Molecular docking studies further corroborated the effective binding of MB-Van1 to the active site of Vanin-1. The docking results indicated that MB-Van1 forms four hydrogen bonds with three amino acids (PRO102, LYS171, and ARG175) in the active site of Vanin-1, with a binding energy of −7.6 kcal/mol, which further confirms the strong interaction between the enzyme and MB-Van1 (Figure S16).

Fluorescence Imaging of Vanin-1 Activity in Living Cells. Prior to applying MB-Van1 in live cell imaging, its cytotoxicity to the LO2 cell line was assessed using the CCK-8 assay. The results indicated that the cell viability of LO2 cells remained above 80% even when the Vanine-1 concentration was as high as 200 μM, demonstrating that MB-Van1 possesses high biocompatibility (Figure S17). In addition, a hemolysis assay was conducted to evaluate the biocompatibility of MB-Van1. The results indicated that even when the probe concentration was as high as 200 μM, the hemolysis rate remained below 4%. This finding demonstrates that MB-Van1 possesses good biocompatibility and is thus suitable for cellular and *in vivo* imaging (Figure S18).

The fluorescence imaging experiments demonstrated that untreated LO2 cells did not exhibit fluorescence. However, upon being treated with MB-Van1, the cells exhibited red fluorescence. To confirm that this fluorescence enhancement was due to endogenous Vanin-1, LO2 cells were treated with RR6, which is a specific inhibitor of Vanin-1. The results demonstrated a significant reduction in fluorescence intensity following RR6 treatment. Subsequently, an inflammatory cell model induced by different concentrations of LPS was established to investigate the changes in Vanin-1 expression within inflammatory cells. The results revealed that as the concentration of LPS increased, the intensity of red fluorescence in the cells significantly escalated, effectively substantiating the overexpression of Vanin-1 in inflammatory cells (Figure 3A,B). Furthermore, Western blot analysis corroborated these findings (Figure 3C).

Fluorescence Imaging of Vanin-1 in an RA Mouse Model. Rheumatoid arthritis (RA) is a chronic autoimmune disorder characterized by persistent inflammation of the synovial tissue.[37] This inflammation extends beyond the joints

https://doi.org/10.1021/acs.analchem.4c05982
Anal. Chem. 2025, 97, 1402−1409

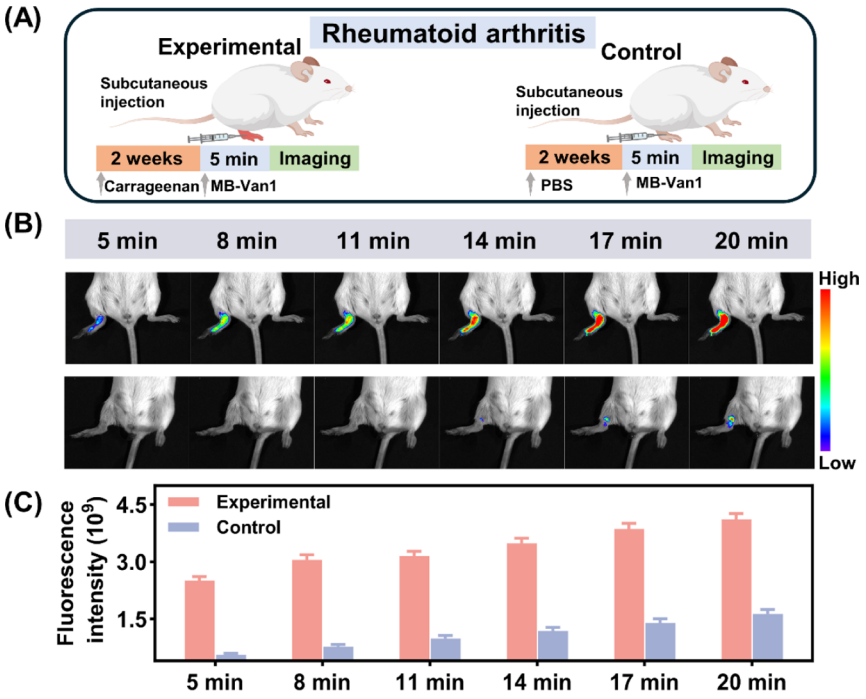

Figure 4. (A) Schematic diagram representing mouse injection and *in vivo* fluorescence imaging. (B) Fluorescence images of mice in the experimental group (top) and control group (bottom) at different times after being injected with MB-Van1. (C) Mean fluorescence intensity of images in (B).

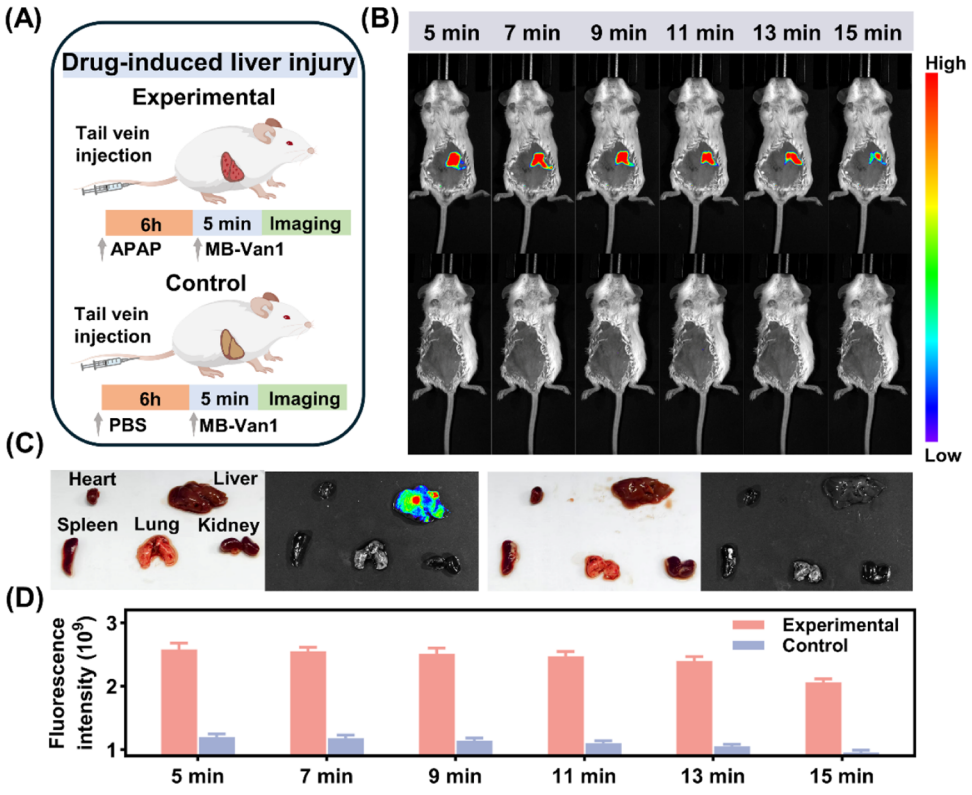

Figure 5. (A) Schematic diagram representing mouse injection and *in vivo* fluorescence imaging. (B) Fluorescence images of mice in the experimental group (top) and control group (bottom) at different times after being injected with MB-Van1. (C) Fluorescence images of dissected organs of mice in the experimental group (left) and control group (right). (D) Mean fluorescence intensity of images in (B).

and progressively erodes surrounding tissues, which can ultimately lead to structural damage and severe functional deterioration.[38] Given the complexity and persistence of the inflammatory response in RA, an in-depth understanding of its molecular mechanisms is essential for effective disease management. Recent studies have identified Vanin-1 as an enzyme playing a pro-inflammatory role in various inflammatory diseases.[21] Considering the distinct pathological features

https://doi.org/10.1021/acs.analchem.4c05982
Anal. Chem. 2025, 97, 1402−1409

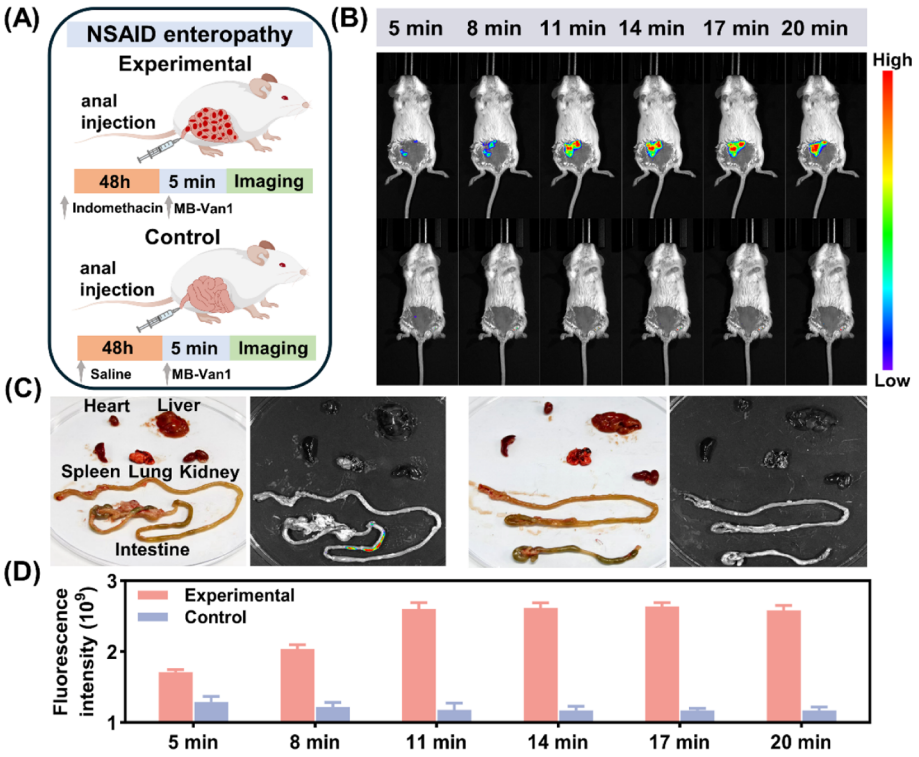

Figure 6. (A) Schematic diagram representing mouse injection and *in vivo* fluorescence imaging. (B) Fluorescence images of mice in the experimental group (top) and control group (bottom) at different times after being injected with MB-Van1. (C) Fluorescence images of dissected organs of mice in the experimental group (left) and control group (right). (D) Mean fluorescence intensity of images in (B).

of RA, it is reasonable to hypothesize that the regulation of Vanin-1 expression in affected joint tissues may be aberrant. To test this hypothesis, MB-Van1 was employed to monitor changes in Vanin-1 levels in a rheumatoid arthritis mouse model. RA was induced in mice using λ-carrageenan, and control mice received an equivalent volume of PBS. After that, MB-Van1 was injected into the joints of both experimental and control mice, and fluorescence imaging was performed 5 min postinjection (Figure 4A). The results demonstrated the joints of RA mice exhibited pronounced fluorescence, whereas those of mice in the control group exhibited minimal fluorescence. This observation indicates that the Vanin-1 expression was significantly upregulated during the pathological progression of RA (Figures 4B,C and S19). This positive correlation suggests that Vanin-1 can serve as a potential biomarker for the diagnosis and monitoring of RA. It also suggests that MB-Van1 has a broad application such as in the studies of other arthritis-related conditions.

Fluorescence Imaging of Vanin-1 in a DILI Mouse Model. Drug-induced liver injury (DILI) is a condition where drugs or their metabolites directly cause liver damage.[39] The pathogenesis of DILI is complex, with oxidative stress being recognized as one of the key contributors to its development.[40] Given the crucial role of Vanin-1 in maintaining intracellular redox homeostasis, we hypothesized that its expression may be altered during the progression of DILI.[21] However, currently, there is a lack of real-time, *in situ* methods to effectively monitor Vanin-1 activity in the liver. To address this gap, we conducted an in-depth study using the MB-Van1 probe in a DILI mouse model induced by acetaminophen (APAP). In the study, mice in the experimental group were administered APAP via intraperitoneal injection to establish the DILI model, while mice in the control group received an equal volume of PBS. Six hours postinjection, both groups of mice were injected with MB-Van1 (10 mM, 100 μL) in the tail vein, and fluorescence imaging was conducted 5 min after the injection (Figure 5A). The results demonstrated a significantly enhanced fluorescence signal in the liver of mice in the experimental group compared to those in the control group. This suggests the Vanin-1 expression was upregulated in the liver during APAP-induced DILI (Figure 5B,D). To further substantiate these findings, the mice were dissected, and their major organs, including the heart, lungs, liver, and kidneys, were collected for *ex vivo* fluorescence imaging. The results revealed only the liver of DILI mice exhibited prominent fluorescence (Figure 5C). This not only confirms the increase in Vanin-1 content in the liver tissue during DILI but also indicates that MB-Van1 is selectively accumulated in the liver. In conclusion, MB-Van1 holds significant potential for real-time monitoring of Vanin-1 activity in the liver. It is an innovative and powerful tool that can be used for the early diagnosis and prognosis of drug-induced liver injury.

Fluorescence Imaging of Vanin-1 in an NSAID Enteropathy Mouse Model. Nonsteroidal anti-inflammatory drugs (NSAIDs) are widely used due to their anti-inflammatory, analgesic, and antipyretic effects.[41] However, their use is also associated with the risk of intestinal damage, which is a condition that often remains asymptomatic until severe symptoms such as ulcers and bleeding manifest.[42] Consequently, the development of early diagnostic methods for NSAID-induced enteropathy has become a critical focus in medicine. The investigations into the mechanisms underlying intestinal inflammation show the distinct pro-inflammatory properties of Vanin-1; and for this reason, it has garnered significant attention. This led us to hypothesize that monitoring changes in Vanin-1 activity could potentially be a

https://doi.org/10.1021/acs.analchem.4c05982
Anal. Chem. 2025, 97, 1402−1409

new approach for the early diagnosis of NSAID-induced intestinal damage. To test this hypothesis, we conducted a confirmatory experiment using the MB-Van1 probe to monitor Vanine-1 a mouse model of enteropathy induced by indomethacin. Mice in the experimental group received indomethacin via gavage, while those in the control group received an equal volume of saline. Following the establishment of the model, both groups of mice were rectally administered with MB-Van1, and fluorescence imaging was performed 5 min postadministration (Figure 6A). The results indicated that the intestinal region of mice in the experimental group showed significant fluorescence, which is in contrast to that of mice in the control group. This observation preliminarily suggests that Vanin-1 may be upregulated during intestinal injury (Figure 6B,D). To further validate these findings, both the experimental and control mice were dissected, and their six major organs, including the intestines, were collected for *ex vivo* fluorescence imaging. The results demonstrated that strong fluorescence was observed exclusively in the intestines of mice in the experimental group, confirming that the Vanin-1 levels in the intestines were elevated during indomethacin-induced enteropathy (Figure 6C). In conclusion, this discovery offers new strategies and hope for the early identification and intervention of NSAID-related enteropathy.

CONCLUSION

In summary, we developed the fluorescent probe MB-Van1 to facilitate real-time monitoring of Vanin-1 activity in inflammatory tissues. This probe not only had excellent optical properties, including nearly zero background fluorescence, but also had high selectivity and sensitivity; all of which enabled the specific detection of Vanin-1 through a dual-mode fluorescence and colorimetric approach. *In vitro* experiments demonstrated that MB-Van1 could quantitatively and sensitively detect Vanin-1. Its detection limit was as low as 0.031 ng/mL in the fluorescence mode and 0.62 ng/mL in the colorimetric mode. We successfully employed MB-Van1 to detect the increased expression of Vanin-1 in LPS-induced LO2 cells. Furthermore, *in vivo* imaging studies revealed that MB-Van1 could rapidly detect the fluorescent-labeled inflammatory tissues, and within only 5 min, it was able to detect the upregulation of Vanin-1 expression in mouse models of drug-induced liver injury, NSAID enteropathy, and rheumatoid arthritis. These findings demonstrate that MB-Van1 can be a powerful new tool for monitoring the dynamic changes of Vanin-1 during inflammation and holds significant potential for applications in mechanistic studies and diagnostic evaluations of other related diseases.

ASSOCIATED CONTENT

Supporting Information

The Supporting Information is available free of charge at https://pubs.acs.org/doi/10.1021/acs.analchem.4c05982.

Additional experimental details, including materials and instruments, determination of the detection limit, enzymatic kinetics assays, molecular docking, CCK8 assay, cell culture, and supplementary figures (PDF)

AUTHOR INFORMATION

Corresponding Authors

Pinyi Ma − *College of Chemistry, Jilin Province Research Center for Engineering and Technology of Spectral Analytical Instruments, Jilin University, Changchun 130012, China;* orcid.org/0000-0002-3230-4928; Email: mapinyi@jlu.edu.cn

Daqian Song − *College of Chemistry, Jilin Province Research Center for Engineering and Technology of Spectral Analytical Instruments, Jilin University, Changchun 130012, China;* orcid.org/0000-0002-4866-1292; Email: songdq@jlu.edu.cn

Authors

Dianfeng Dai − *College of Chemistry, Jilin Province Research Center for Engineering and Technology of Spectral Analytical Instruments, Jilin University, Changchun 130012, China*

Zhimin Zhang − *Department of Pharmacy, Changchun Medical College, Changchun 130031, China*

Mo Ma − *College of Chemistry, Jilin Province Research Center for Engineering and Technology of Spectral Analytical Instruments, Jilin University, Changchun 130012, China; School of Pharmacy, Jilin University, Changchun 130012, China*

Jingkang Li − *College of Chemistry, Jilin Province Research Center for Engineering and Technology of Spectral Analytical Instruments, Jilin University, Changchun 130012, China*

Siqi Zhang − *College of Chemistry, Jilin Province Research Center for Engineering and Technology of Spectral Analytical Instruments, Jilin University, Changchun 130012, China*

Complete contact information is available at: https://pubs.acs.org/10.1021/acs.analchem.4c05982

Notes

The authors declare no competing financial interest.

ACKNOWLEDGMENTS

This work was supported by the National Natural Science Foundation of China (22074052 and 22004046) and the Science and Technology Developing Foundation of Jilin Province of China (20230204116YY).

REFERENCES

(1) Li, G.; Zhang, L.; Zheng, H.; Lin, W. *Coord. Chem. Rev.* **2024**, *517*, 215975.

(2) Furman, D.; Campisi, J.; Verdin, E.; Carrera-Bastos, P.; Targ, S.; Franceschi, C.; Ferrucci, L.; Gilroy, D. W.; Fasano, A.; Miller, G. W.; Miller, A. H.; Mantovani, A.; Weyand, C. M.; Barzilai, N.; Goronzy, J. J.; Rando, T. A.; Effros, R. B.; Lucia, A.; Kleinstreuer, N.; Slavich, G. M. *Nat. Med.* **2019**, *25*, 1822−1832.

(3) Klein, R. S.; Hunter, C. A. *Immunity* **2017**, *46*, 891−909.

(4) Peña, O. A.; Martin, P. *Nat. Rev. Mol. Cell Biol.* **2024**, *25*, 599−616.

(5) Klotz, L.; Antel, J.; Kuhlmann, T. *Nat. Rev. Neurol.* **2023**, *19*, 305−320.

(6) Sands, B. E. *Gastroenterology* **2015**, *149*, 1275−1285.

(7) Wang, X.; Ding, Q.; Groleau, R. R.; Wu, L.; Mao, Y.; Che, F.; Kotova, O.; Scanlan, E. M.; Lewis, S. E.; Li, P.; Tang, B.; James, T. D.; Gunnlaugsson, T. *Chem. Rev.* **2024**, *124*, 7106−7164.

(8) Heneka, M. T.; Carson, M. J.; El Khoury, J.; Landreth, G. E.; Brosseron, F.; Feinstein, D. L.; Jacobs, A. H.; Wyss-Coray, T.; Vitorica, J.; Ransohoff, R. M.; et al. *Lancet Neurol.* **2015**, *14*, 388−405.

(9) Yamamoto, T.; Kawada, K.; Obama, K. *Int. J. Mol. Sci.* **2021**, *22*, 8002.

(10) Calabrese, M.; Magliozzi, R.; Ciccarelli, O.; Geurts, J. J. G.; Reynolds, R.; Martin, R. *Nat. Rev. Neurosci.* **2015**, *16*, 147−158.
(11) Xu, S. L.; Yan, K. C.; Xu, Z. H.; Wang, Y.; James, T. D. *Chem. Soc. Rev.* **2024**, *53*, 7590−7631.
(12) Geng, Y. J.; Wang, Z.; Zhou, J. Y.; Zhu, M. G.; Liu, J.; James, T. D. *Chem. Soc. Rev.* **2023**, *52*, 3873−3926.
(13) Yang, M. W.; Fan, J. L.; Du, J. J.; Peng, X. J. *Chem. Sci.* **2020**, *11*, 5127−5141.
(14) Cui, W. L.; Wang, M. H.; Yang, Y. H.; Wang, J. Y.; Zhu, X. Z.; Zhang, H. T.; Ji, X. X. *Coord. Chem. Rev.* **2023**, *474*, 214848.
(15) Han, H. H.; Tian, H.; Zang, Y.; Sedgwick, A. C.; Li, J.; Sessler, J. L.; He, X. P.; James, T. D. *Chem. Soc. Rev.* **2021**, *50*, 9391−9429.
(16) Niu, H. Y.; Liu, J. W.; O'Connor, H. M.; Gunnlaugsson, T.; James, T. D.; Zhang, H. *Chem. Soc. Rev.* **2023**, *52*, 2322−2357.
(17) Huang, J. G.; Pu, K. Y. *Angew. Chem., Int. Ed.* **2020**, *59*, 11717−11731.
(18) Pitari, G.; Malergue, F.; Martin, F.; Philippe, J. M.; Massucci, M. T.; Chabret, C.; Maras, B.; Duprè, S.; Naquet, P.; Galland, F. *FEBS Lett.* **2000**, *483*, 149−154.
(19) Aurrand-Lions, M.; Galland, F.; Bazin, H.; Zakharyev, V. M.; Imhof, B. A.; Naquet, P. *Immunity* **1996**, *5*, 391−405.
(20) Ling, L.; Lu, H. T.; Wang, H. F.; Shen, M. J.; Zhang, H. B. *Kidney Blood Pressure Res.* **2019**, *44*, 565−582.
(21) Bartucci, R.; Salvati, A.; Olinga, P.; Boersma, Y. L. *Int. J. Mol. Sci.* **2019**, *20*, 3891.
(22) Washino, S.; Hosohata, K.; Oshima, M.; Okochi, T.; Konishi, T.; Nakamura, Y.; Saito, K.; Miyagawa, T. *Int. J. Mol. Sci.* **2019**, *20*, 899.
(23) Hosohata, K.; Ando, H.; Fujimura, A. *J. Pharmacol. Exp. Ther.* **2012**, *341*, 656−662.
(24) Hosohata, K.; Ando, H.; Fujiwara, Y.; Fujimura, A. *Toxicology* **2011**, *290*, 82−88.
(25) Berruyer, C.; Pouyet, L.; Millet, V.; Martin, F. M.; LeGoffic, A.; Canonici, A.; Garcia, S.; Bagnis, C.; Naquet, P.; Galland, F. *J. Exp. Med.* **2006**, *203*, 2817−2827.
(26) Roisin-Bouffay, C.; Castellano, R.; Valero, R.; Chasson, L.; Galland, F.; Naquet, P. *Diabetologia* **2008**, *51*, 1192−1201.
(27) Yamashita, N.; Yashiro, M.; Ogawa, H.; Namba, H.; Nosaka, N.; Fujii, Y.; Morishima, T.; Tsukahara, H.; Yamada, M. *Biochem. Bioph. Res. Commun.* **2017**, *489*, 466−471.
(28) Boersma, Y. L.; Newman, J.; Adams, T. E.; Cowieson, N.; Krippner, G.; Bozaoglu, K.; Peat, T. S. *Acta Crystallogr., Sect. D: Biol. Crystallogr.* **2014**, *70*, 3320−3329.
(29) Yu, H.; Cui, Y. Y.; Guo, F. Y.; Zhu, Y. T.; Zhang, X. A.; Shang, D.; Dong, D. S.; Xiang, H. *Eur. J. Pharmacol.* **2024**, *962*, 176220.
(30) Nitto, T.; Onodera, K. *J. Pharmacol. Sci.* **2013**, *123*, 1−8.
(31) Schalkwijk, J.; Jansen, P. *Biochem. Soc. Trans.* **2014**, *42*, 1052−1055.
(32) Yang, Y. T.; Hu, Y. M.; Shi, W.; Ma, H. M. *Chem. Sci.* **2020**, *11*, 12802−12806.
(33) Li, J. X.; Ma, M.; Li, J. K.; Xu, L. L.; Song, D. Q.; Ma, P. Y.; Fei, Q. *Anal. Chem.* **2023**, *95*, 17577−17585.
(34) Feng, Y. R.; Xu, S.; Guo, H. W.; Ren, T. B.; Huan, S. Y.; Yuan, L.; Zhang, X. B. *Anal. Chem.* **2023**, *95*, 14754−14761.
(35) Fujita, K.; Urano, Y. *Chem. Rev.* **2024**, *124*, 4021−4078.
(36) van Manen, L.; Handgraaf, H. J. M.; Diana, M.; Dijkstra, J.; Ishizawa, T.; Vahrmeijer, A. L.; Mieog, J. S. D. *J. Surg. Oncol.* **2018**, *118*, 283−300.
(37) Yap, H. Y.; Tee, S. Z. Y.; Wong, M. M. T.; Chow, S. K.; Peh, S. C.; Teow, S. Y. *Cells* **2018**, *7*, 161.
(38) Brown, A. K.; Conaghan, P. G.; Karim, Z.; Quinn, M. A.; Ikeda, K.; Peterfy, C. G.; Hensor, E.; Wakefield, R. J.; O'Connor, P. J.; Emery, P. *Arthritis Rheumatol.* **2008**, *58*, 2958−2967.
(39) Ramachandran, A.; Jaeschke, H. *Semin. Liver Dis.* **2019**, *39*, 221−234.
(40) Li, S.; Tan, H. Y.; Wang, N.; Zhang, Z. J.; Lao, L. X.; Wong, C. W.; Feng, Y. B. *Int. J. Mol. Sci.* **2015**, *16*, 26087−26124.
(41) Parolini, M. *Sci. Total Environ.* **2020**, *740*, 140043.
(42) Bjarnason, I.; Scarpignato, C.; Holmgren, E.; Olszewski, M.; Rainsford, K. D.; Lanas, A. *Gastroenterology* **2018**, *154*, 500−514.

https://doi.org/10.1021/acs.analchem.4c05982
Anal. Chem. 2025, 97, 1402−1409